

Shifted excitation Raman difference spectroscopy for soil component identification and soil carbonate determination in the presence of strong fluorescence interference

Kay Sowoidnich¹  | Martin Maiwald¹  | Markus Ostermann²  |
Bernd Sumpf¹ 

¹Ferdinand-Braun-Institut, Leibniz-Institut für Höchstfrequenztechnik, Berlin, Germany

²Federal Institute for Materials Research and Testing (BAM), Berlin, Germany

Correspondence

Kay Sowoidnich, Ferdinand-Braun-Institut, Leibniz-Institut für Höchstfrequenztechnik, Gustav-Kirchhoff-Straße 4, 12489 Berlin, Germany.
Email: kay.sowoidnich@fbh-berlin.de

Funding information

Federal Ministry of Education and Research, Grant/Award Numbers: 031B0513C, 16FMD02

Abstract

Detailed knowledge about soil composition is an important prerequisite for many applications, for example precision agriculture. Current standard laboratory methods are complex and time-consuming but could be complemented by non-invasive optical techniques. Its capability to provide a molecular fingerprint of individual soil components makes Raman spectroscopy a very promising candidate. A major challenge is strong fluorescence interference inherent to soil, but this issue can be overcome effectively using shifted excitation Raman difference spectroscopy (SERDS). A customized dual-wavelength diode laser emitting at 785.2 and 784.6 nm was used to investigate 117 soil samples collected from an agricultural field along a distance of 624 m and down to depths of 1 m. To address soil spatial heterogeneity, a raster scan approach comprising 100 measurement spots per sample was applied. Based on the Raman spectroscopic fingerprint extracted from intense fluorescence interference by SERDS, 13 mineral soil constituents were identified, and even closely related molecular species could be discriminated, for example polymorphs of titanium dioxide and calcium carbonate. For the first time, the capability of SERDS is demonstrated to predict the calcium carbonate content as an important soil parameter using partial least squares regression ($R^2 = 0.94$, root mean square error of cross-validation RMSECV = 2.1%). Our findings demonstrate that SERDS can extract a wealth of spectroscopic information from disturbing backgrounds enabling qualitative and quantitative soil analysis. This highlights the large potential of SERDS for precision agriculture but also in further application areas, for example geology, cultural heritage and planetary exploration.

KEYWORDS

calcium carbonate, dual-wavelength diode laser, fluorescence rejection, shifted excitation Raman difference spectroscopy, soil minerals

This is an open access article under the terms of the [Creative Commons Attribution](https://creativecommons.org/licenses/by/4.0/) License, which permits use, distribution and reproduction in any medium, provided the original work is properly cited.

© 2023 The Authors. *Journal of Raman Spectroscopy* published by John Wiley & Sons Ltd.

1 | INTRODUCTION

Precision agriculture^[1] and effective soil nutrient management are becoming increasingly important to improve crop productivity, increase overall soil health, and reduce excessive use of commercial fertilizers. Established standard laboratory methods for soil analysis are complex, time-consuming and labor-intensive making the analysis of larger areas with high spatial resolution difficult,^[2] but they could be complemented by non-invasive optical measurement approaches. Such techniques, ideally with the ability to be applied on-site without the need for sample preparation, have the potential to provide necessary information for evidence-based decision support systems.^[3] Raman spectroscopy is a powerful spectroscopic tool that provides a fingerprint on a molecular level thus enabling qualitative and quantitative sample analysis. The technique has thus a great potential for soil compositional analysis but, despite a wide range of potential applications, to date is still largely underexplored in this area.

The major reason for the scarce use of Raman spectroscopy is the interference of fluorescence^[4] mainly arising from soil organic matter^[5,6] and clay minerals.^[7,8] In some cases, strong fluorescence can even prevent successful Raman analysis of soil samples.^[9] One approach to mitigate this issue is to use confocal Raman microscopy to reduce the amount of out-of-focus fluorescence contributions being detected. Micro-Raman studies have been reported exemplarily for soil analysis in a forensic context^[10] and for the analysis of soil minerals.^[11] However, Raman microscopic investigations conducted by our group have demonstrated that residual fluorescence interference is still an issue potentially masking weak Raman signals even when a confocal geometry is chosen.^[5,12]

Due to the severity of fluorescence interference in many cases, additional approaches were required to extract useful Raman spectroscopic information from soil specimens. One of the simplest techniques is a mathematical removal of background contributions as applied for the analysis of Chinese farmland soils,^[13] soil characterization at archeological sites^[14] and the identification of phosphates in soil.^[15] Such mathematical post-processing of Raman spectra may be applicable for moderate fluorescence interference, but our previous work in the case of highly fluorescent soil specimens has shown its limitations, for example when using polynomial background subtraction.^[16] Furthermore, these techniques are unable to adequately separate Raman signals from non-Raman spectral features, for example fixed pattern noise or artefacts, limiting their applicability in case of low signal levels.

Another technique is fluorescence bleaching, that is the reduction of the fluorescence intensity by exposing the sample to laser radiation before starting the actual spectral acquisition. This has been applied for the characterization of Hawaiian soils^[17] and for explosives detection within soil.^[18] A serious drawback of this method is that heating, modification and even damage to the sample due to prolonged exposure to the laser beam cannot be ruled out. Another detrimental effect is related to the extended amount of time required for the measurements due to the bleaching time, which can take up to 20% of the time used to record the Raman spectra.^[18]

An instrumental method to address fluorescence interference is the usage of shorter excitation wavelengths in the ultraviolet (UV) spectral range. Although the studies mentioned so far have applied laser wavelengths of 785, 532 or 514.5 nm, an excitation in the UV can be beneficial. This has been reported using a laser emitting at 325 nm to classify five types of Brazilian soil but residual background contributions were still present requiring an additional baseline subtraction.^[19] To fully exploit the benefits of this approach, deep-UV Raman spectroscopy with excitation wavelengths below 250 nm should be applied. This enables to efficiently separate the spectral region containing the Raman signals from the spectral range where fluorescence emission occurs. Deep-UV Raman spectroscopy using 244 nm excitation has been demonstrated for the analysis of phosphorous compounds in different soils.^[20] Unfortunately, due to the high-energetic laser photons, most of the organic material within the soil decomposed during the Raman measurements, in some cases, even when strong sample cooling to -100°C was applied.^[20]

Shifted excitation Raman difference spectroscopy (SERDS)^[21,22] is another very promising approach to address the fluorescence issue and our group evaluates the potential of this technique for soil inspection. Based on the consecutive excitation of the sample at two slightly different laser wavelengths, SERDS is a powerful physical approach to extracting the characteristic molecular fingerprint of a specimen from interferences. The Raman signals will directly follow the small shift in excitation wavelength (e.g. 0.6 nm at 785 nm), whereas backgrounds remain essentially unchanged. Subtracting both recorded Raman spectra can then effectively separate the characteristic molecular fingerprint of the sample from background interferences caused by fluorescence and also ambient lights.^[23,24] We have recently demonstrated that SERDS can successfully be applied for the qualitative investigation of soil enabling the identification of quartz, feldspar and hydroxyapatite^[12] as well as for the determination of the soil organic matter content.^[16]

In this paper, we present systematic SERDS investigations for the characterization of 117 soil samples collected from an agricultural field. To address soil spatial heterogeneity at multiple length scales, a raster scan approach comprising 100 measurement spots per sample was applied to the specimens collected from a two-dimensional cross-section along a distance of 624 m and down to a depth of 1 m. This allowed to incorporate topsoil samples that are affected by agricultural machining (ca. 0–40 cm depth) as well as subsoil samples that remain mostly unaffected (ca. 40–100 cm depth). The SERDS spectra enabled us to detect and identify 13 major and minor soil constituents enabling the discrimination of even closely related molecular species within soil including polymorphic forms. For the first time, multivariate regression of representative average spectra of the 117 topsoil and subsoil specimens could successfully be used for the quantification of the soil calcium carbonate content, an important parameter in the context of liming requirements.

2 | MATERIALS AND METHODS

2.1 | Experimental setup for shifted excitation Raman difference spectroscopy

For our experiments, a compact laboratory setup for shifted excitation Raman difference spectroscopy has been developed and is described in detail in our previous study.^[16] Briefly, the excitation light of an in-house developed 785 nm dual-wavelength diode laser^[25] passes through an optical isolator with 60 dB blocking (FI-780-5TVC, Qioptiq) and is then focused into an optical fiber with a core diameter of 100 μm (LEONI Fiber Optics). After collimation at the fiber output, the laser light passes two bandpass filters (LL01-785-25, Semrock) and is reflected at a Raman long-pass filter (DI02-R785-25x36, Semrock) and a silver mirror (Qioptiq). Subsequently, an achromatic lens with a focal length of 30 mm and a diameter of 25.4 mm (Thorlabs) focuses the laser light through a sapphire window (Newport corporation) onto the soil sample with a spot size of approximately 100 μm . Automatic probing of the sample at selected points in a grid pattern is realized by a motorized X–Y stage with a positioning accuracy of 4 μm (TRA12CC, Newport corporation).

The back-scattered light emerging from the specimen is collected by the same lens used for focusing the laser light. Following reflection at the silver mirror and transmission through a set of three Raman long-pass filters (DI02-R785-25x36 and LP02-785RU-25, Semrock), the Raman Stokes scattered light is launched into an optical

fiber with a core diameter of 200 μm (Thorlabs). This fiber transfers the light towards the spectrometer (optical resolution of 4 cm^{-1} , Tornado U1, Tornado Spectral Systems) with an attached charge-coupled device detector (MityCCD H10141, CriticalLink) that is thermoelectrically cooled down to -10°C . Adjustment of the laser operation parameters, recording of the Raman spectra and control of the motorized sample stage are realized by in-house written software.

2.2 | Sample material and X-ray fluorescence analyses

For our study, 117 soil samples were exemplarily collected from the topsoil and subsoil layers (down to 100 cm depth) of an agricultural field in northeast Germany (Latitude: 52.394316 N; Longitude: 14.461156E) in 2020. Additional information about selected soil parameters of the field can be found elsewhere.^[16] From previous investigations, it is well known that the field possesses a pronounced spatial variability and samples were taken accordingly along a line across the field covering a total distance of 624 m with adjacent points being separated by 24 m. At each of the 27 probed locations, samples were collected from up to five different depth ranges, namely 0–20, 20–40, 40–60, 60–80 and 80–100 cm to assess soil layers strongly affected by agricultural machining as well as those layers that remain mainly unaffected. In line with sample preparation standards in soil science, the specimens were air-dried at room temperature and sieved to grain sizes smaller than 2 mm before further analysis. Samples were divided into multiple sub-sets, where one was used for the SERDS experiments and another one for the X-ray fluorescence (XRF) reference analyses.

X-ray fluorescence measurements were performed using a Panalytical MagiX Pro wavelength dispersive spectrometer equipped with a 4 kW water-cooled tube. Soil samples were placed as loose powder in X-ray sample cups covered with a 6 μm thick X-ray Mylar[®] film and measured under a helium atmosphere. The application was calibrated with 16 certified reference soil materials (CRM) from different institutions: GBW07402 and GBW07405 from the National Research Centre for Certified Reference Materials (Beijing, China); NCS DC73023, NCS DC73030, NCS DC85109 and NCS DC87104 from the National Analysis Centre for Iron and Steel (Beijing, China); TILL1, TILL2 and TILL3 from the Canadian Centre for Mineral and Energy Technology—CANMET (Ottawa, Canada); BAM-U110 from the Federal Institute for Materials Research and Testing—BAM; Soil-5 from the International Atomic Energy Agency—IAEA (Vienna, Austria); VS2498–83 from the ICRM Centre

(Moscow, Russia); NIST1646a, NIST2704, NIST2709 and NIST2710 from the National Institute of Standards and Technology—NIST (Gaithersburg, USA).

2.3 | SERDS measurement parameters

The SERDS experiments were conducted with the soil samples being located in round aluminum cups (diameter 30 mm × depth 7.6 mm) and covered with a sapphire window to obtain a flat sample surface. The specimens were mounted in a motorized X–Y stage and probed at 100 positions in a 10 × 10-point grid pattern with 1.1 mm spacing between grid points thus covering an area of 1 cm². At each spot, 10 single Raman spectra with an accumulation time of 1 s were recorded for both excitation wavelengths using an optical power at the sample position of 20 mW.

2.4 | Processing of SERDS spectra

The data processing for SERDS is detailed in our previous publication,^[16] and only a brief overview will be given here. Using an in-house developed algorithm implemented in MATLAB (R2017a, MathWorks, Natick, MA, USA), initially, the SERDS difference spectrum was calculated from the mean Raman spectra recorded at each excitation wavelength. Following cubic spline fitting to generate a zero-baseline-centred derivative-shaped difference spectrum, a numerical integration is performed to obtain a reconstructed SERDS spectrum in a conventional form. The last step comprises a baseline correction of the reconstructed SERDS spectrum to achieve a straight horizontal baseline. For qualitative analysis, the obtained SERDS spectra were assessed individually for the identification of soil constituents. For each sample, outliers were removed if their SERDS intensity was above an empirically determined threshold of four times the mean intensity of the spectra recorded at the 100 different locations.^[16] In the case of quantitative analysis, the average of the remaining spectra was calculated to obtain one representative mean spectrum for each specimen to consider the inherent soil heterogeneity.

2.5 | Data analysis

In case of qualitative soil analysis aiming for the identification of individual constituents present in the investigated specimens, the following approach was used. As a first selection criterion, individual SERDS spectra showing strong characteristic Raman signals of the respective target

substance (e.g. quartz, feldspar, calcite etc.) were identified by visual inspection. Aiming to obtain mostly “pure” SERDS spectra of selected soil constituents, a second selection criterion was applied. This is that the selected spectra should exhibit pronounced Raman signals of the respective target substance but also display minimal interference from Raman signals of other soil constituents (e.g. quartz as frequently present mineral). Based on this procedure, the three “purest” SERDS spectra with strong Raman signals of the target substance were chosen and their average was calculated. As only two SERDS spectra showing the clear presence of diopside were detected, only these two spectra (rather than three as for the other constituents) were averaged. These data (normalized to the respective maximum intensity value and vertically offset for clarity) are then presented in Figure 2.

For all univariate and multivariate analyses, the data set containing average spectra for each of the 117 soil samples has been normalized to the intensity of the Raman signal at 749 cm⁻¹, originating from the sapphire measurement window. In a first attempt, calcium carbonate Raman signal intensities were determined by using mean values of three points each around 1084 and 711 cm⁻¹ above zero baseline. When considering both characteristic Raman signals, the sum of the intensities of the two signals is used.

For comparison, the cumulative intensities of 17 points in the range 1076–1093 cm⁻¹ (Raman signal at 1084 cm⁻¹), 12 points in the range 705–717 cm⁻¹ (Raman signal at 711 cm⁻¹) or the sum of intensities in both of these regions (Raman signals at 1084 cm⁻¹ and 711 cm⁻¹) were calculated. In all cases, the Raman signal intensities were correlated with reference calcium carbonate contents as derived from soil calcium contents determined by XRF analysis.

Prior to multivariate regression aiming for the quantification of calcium carbonate content, SERDS spectra were truncated to two different spectral regions to assess the effects of the inclusion or the exclusion of the major carbonate Raman signal at 1084 cm⁻¹. In both cases, the major quartz Raman signal located at 465 cm⁻¹ was excluded from the analyzed spectral range as pronounced variations in its signal intensity do not correlate with the calcium carbonate content thus leading to decreased model performance. The first region comprising the 500–1100 cm⁻¹ range was selected as it contains both characteristic Raman signals of the target substance at 1084 and 711 cm⁻¹ but excludes the strong quartz Raman signal located at 465 cm⁻¹. In the second case, the spectral region was further narrowed to 500–1040 cm⁻¹ to evaluate modeling performance if the main Raman signal of the target substance at 1084 cm⁻¹ is not considered (see Figure 2 for Raman spectra of soil constituents). For the

partial least squares (PLS) regression of the SERDS data against calcium carbonate contents calculated from soil calcium contents determined by XRF, the MATLAB function “plsregress” included in the Statistics and Machine Learning Toolbox and based on the SIMPLS algorithm^[26] was applied. Considering the sample size of 117 spectra, 10-fold cross-validation was chosen as a suitable cross-validation approach.

The included maximum number of PLS components in the regression models has been identified by calculating the model root mean square error of cross-validation (RMSECV) as a function of the number of components. The common practice in multivariate regression is then to select the number of components giving the minimum RMSECV.^[27] Care must however be taken not to include insignificant information, for example noise, into the model. To address this issue, a further selection criterion has been applied in our case. From the maximum number of components defined by the minimum RMSECV, only those components that explained more than 1% variation in the response variables, that is the reference calcium carbonate contents, were included in the partial least squares regression (PLSR) models.

3 | RESULTS AND DISCUSSION

3.1 | Influence of soil heterogeneity on detected spectra

In the case of micro-Raman spectroscopy with spot sizes on the order of a few micrometers, identification of individual soil constituents is rather easy as for each measurement spot mostly pure component spectra can be acquired.^[5,11,12,17] It should be noted that in our study, an excitation and collection spot size of approximately 100 μm has been selected to average out soil spatial heterogeneities on the micrometer scale. The recorded spectra from individual measurement spots will thus very likely contain molecule-specific information from more than a single species in most cases. Nevertheless, in the following, it will be demonstrated that the molecule-specific information extracted from intense background contributions by means of SERDS can successfully be applied for a qualitative soil analysis to identify the presence of individual constituents.

3.2 | SERDS for identification of soil constituents

In our previous work, we have shown that SERDS can successfully be applied for the identification of selected

inorganic (quartz, feldspar, anatase, calcite and hydroxyapatite) and organic (amorphous carbon) soil constituents.^[12,16] The present investigation is now going a step further by discriminating even closely related molecular species within soil including polymorphic forms.

As an example, the averaged 10 single Raman spectra recorded for each excitation wavelength (784.6 and 785.2 nm) from a single measurement spot of one selected soil sample are shown in Figure 1 (top curves). Due to strong fluorescence interference, virtually no Raman signals of soil constituents except for quartz (SiO_2) at 465 cm^{-1} ^[28] can be observed. The spectral shift of the quartz Raman signal following the applied shift in excitation wavelength of 0.6 nm (corresponding to 10 cm^{-1}) can be recognized when comparing the two Raman spectra. Application of SERDS according to the procedure described above can reveal additional spectroscopic information from the Raman data. Due to the underlying physical approach, the

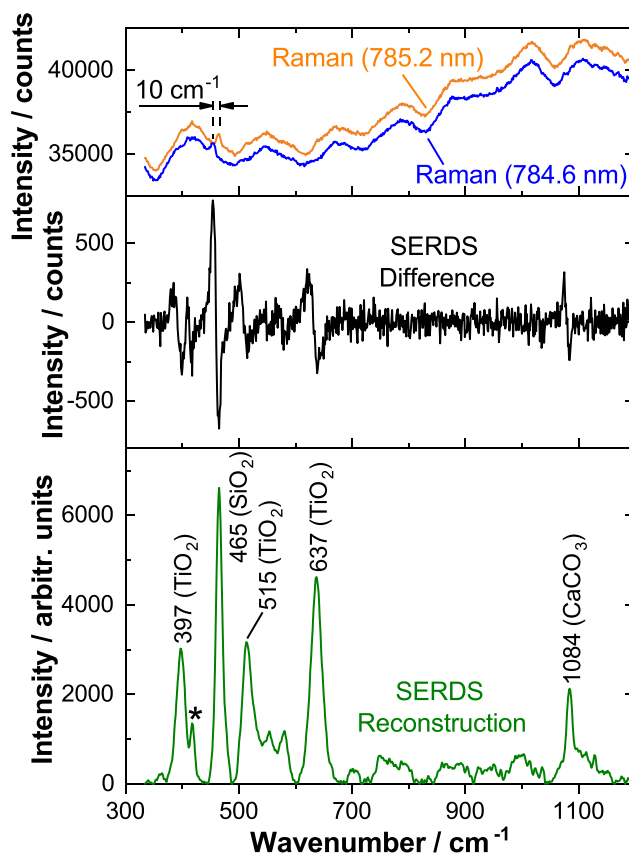


FIGURE 1 Average of 10 Raman spectra (top curves) excited at 785.2 and 784.6 nm, SERDS difference spectrum (centre curve) and reconstructed SERDS spectrum (bottom curve) obtained from one single measurement position of a selected soil sample. Asterisk indicates the Raman signal originating from the sapphire window. [Colour figure can be viewed at wileyonlinelibrary.com]

SERDS difference spectrum displayed in the center of Figure 1 effectively separates Raman signals (present as derivative-like structures) from interfering contributions, for example fluorescence. In this way, the presence of further Raman signal beside the major quartz signal becomes evident.

The reconstructed SERDS spectrum (bottom curve in Figure 1) provides a smoothing of the SERDS difference spectrum due to the applied numerical integration thus allowing for even better identification of several characteristic Raman signals. A contribution from the sapphire window used to cover the soil sample in the experimental setup is indicated by an asterisk and can be found at 418 cm^{-1} .^[29,30] Furthermore, Raman signals of the mineral soil components anatase (TiO_2) at 397, 515 and 637 cm^{-1} ^[31] and calcite (CaCO_3) at 1084 cm^{-1} ^[11] can be identified. SERDS could thus successfully be applied to recover Raman spectroscopic information from strong fluorescence interference in soil enabling the detection of selected soil constituents.

In the next step, representative SERDS spectra of mineral soil components identified within our investigated set of soil samples will be presented. As outlined above, these spectra were calculated as averages of SERDS spectra from three measurement spots for each component (except for diopside with only two spots being averaged). The selection criteria of spectra for averaging were strong Raman signal intensity of the target substance and minimal spectral interference from Raman signals of other soil constituents. These data could serve as a useful collection of reference spectra in terms of substance identification for further SERDS studies on soils, for example for mineral classification applying multivariate analyses.^[32,33]

3.2.1 | Silicates

Among various soil constituents, silicate minerals are of particular interest due to their relative abundance and importance.^[34] Representative average SERDS spectra obtained from selected silicates are displayed in Figure 2A. The asterisks indicate Raman signals at 418 and 750 cm^{-1} that are not due to intrinsic soil constituents but rather originating from the sapphire window that is used to cover the soil samples during the measurement.^[29,30] In the case of quartz (SiO_2) as the major component of main types of soil, the strongest Raman signal due to the Si–O–Si symmetric stretching vibration is located at 465 cm^{-1} , whereas another weak Raman signal attributed to a lattice mode at 356 cm^{-1} can be identified as well.^[28]

In case of feldspar, Na- and K-rich modifications can be recognized. The Na-feldspar ($\text{NaAlSi}_3\text{O}_8$) is characterized by two prominent Raman signals at 480 and 509 cm^{-1} , whereas the K-feldspar (KAlSi_3O_8) has its two major Raman signals located at 475 and 513 cm^{-1} . In both cases, these bands are due to the breathing modes of the four-membered tetrahedral rings.^[35–38] For K-feldspar, two additional weak signals at 375 and 402 cm^{-1} that are specific to that modification could be observed.^[35,38] As both of the strongest feldspar Raman signals shift in opposite directions with composition, a reliable detection of the actual feldspar phase can be realized. Identification is eased in this case as no strong contributions from quartz are present as an intense quartz signal at 465 cm^{-1} could partially overlap with the feldspar Raman signals located in the range 475 – 480 cm^{-1} . Nevertheless, on the condition that the spectral resolution of the applied Raman instrument is sufficiently high, a discrimination between feldspar

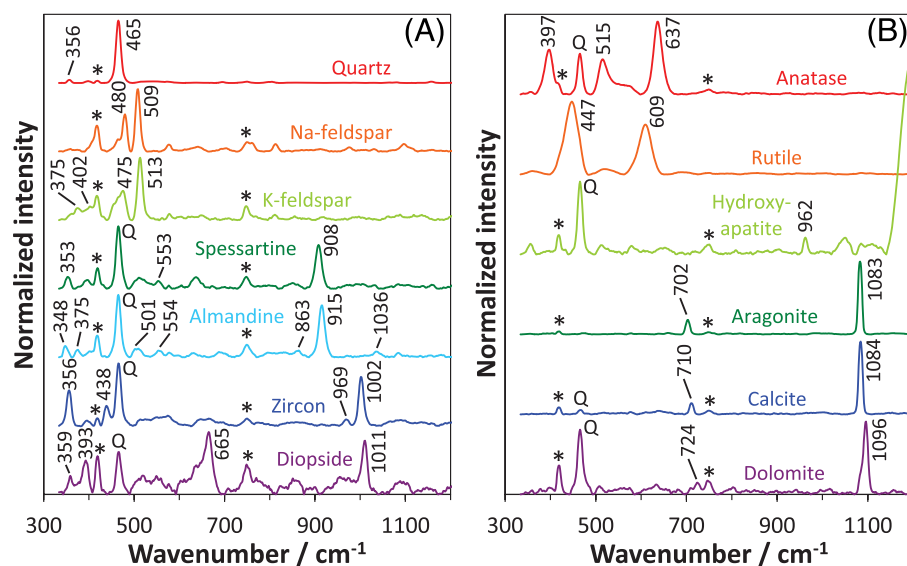


FIGURE 2 Averaged SERDS spectra of identified soil constituents. Each spectrum is calculated as the average of three measurement positions, except for diopside, where only two spots were averaged. Asterisks indicate Raman signals of the sapphire measurement window, whereas the letter “Q” denotes contributions from quartz in spectra of other soil constituents. Spectra are normalized to their respective maximum value in the range 340 – 1100 cm^{-1} and are vertically offset for clarity. [Colour figure can be viewed at wileyonlinelibrary.com]

endmembers should, in principle, also be possible only based on the Raman signal around 510 cm^{-1} .

Two members of the garnet group could be recognized in the recorded soil SERDS spectra, namely spessartine ($\text{Mn}_3\text{Al}_2\text{Si}_3\text{O}_{12}$) and almandine ($\text{Fe}_3\text{Al}_2\text{Si}_3\text{O}_{12}$). In case of spessartine, three characteristic Raman signals can be recognized in the SERDS spectrum. The strongest band due to the Si–O symmetric stretching mode can be found at 908 cm^{-1} . Two weaker Raman signals are located at 553 and 353 cm^{-1} and correspond to the O–Si–O symmetric bending mode and SiO_4 rotation, respectively.^[39–41] Almandine as another garnet with different composition has its Si–O symmetric stretching vibration located at 915 cm^{-1} . Furthermore, weaker bands at 863 and 1036 cm^{-1} due to O–Si–O asymmetric stretching, at 554 cm^{-1} attributed to O–Si–O symmetric bending vibrations and at 501 cm^{-1} due to O–Si–O asymmetric bending vibrations can be identified. Towards the lower end of the investigated spectral range, two Raman signals assigned to SiO_4 tetrahedron rotations are observed at 348 and 375 cm^{-1} .^[28,40,42,43]

Zircon (ZrSiO_4) could be detected as well based on its characteristic Raman spectroscopic signature. The strongest Raman signal is observed at 1002 cm^{-1} due to the antisymmetric stretching mode of SiO_4 tetrahedra. Another prominent signal assigned to an external rotation mode is located at 356 cm^{-1} . Two weaker Raman bands at 438 and 969 cm^{-1} are attributed to the symmetric bending vibration and symmetric stretching vibration of SiO_4 , respectively.^[44–46] It should be noted that the Raman signal positions of natural zircon as observed in our study are slightly different from those of highly crystalline zircon^[47] due to structural changes associated with radiation damage. This effect becomes evident by the broadening of Raman signals and shifting of Raman signal positions towards lower wavenumbers.^[46,48]

The last silicate that has been detected is diopside ($\text{CaMgSi}_2\text{O}_6$) and its average SERDS spectrum is displayed in the bottom part of Figure 2A. The strong Raman signal at 1011 cm^{-1} is due to the symmetric Si–O stretching vibrations within the SiO_4 tetrahedron, whereas another intense contribution from a mixed stretching bending mode of the Si–O–Si bridging bond can be observed at 665 cm^{-1} . The two remaining Raman signals at 359 and 393 cm^{-1} are attributed to modes involving Ca–O and Mg–O bending and stretching vibrations.^[49–51]

3.2.2 | Titanium dioxides

Besides the various silicate species, a number of other substances were detected in the soil specimens using

SERDS and their spectra are presented in Figure 2B. Titanium dioxide exists in several polymorphic forms that have the same chemical composition (TiO_2) but exhibit different molecular arrangements within their crystal structure.^[52] Due to the molecular fingerprint obtained by Raman spectroscopy and SERDS, a clear distinction between these polymorphs can be achieved. This is exemplarily shown in the top part of Figure 2B. The anatase polymorph of TiO_2 is characterized by three prominent Raman signals. The symmetric Ti–O stretching vibration is located at 637 cm^{-1} , whereas O–Ti–O bending vibrational bands can be observed at 397 and 515 cm^{-1} . A more precise assignment of the bending vibrations cannot be given at this point as there is still some debate about the contributions of symmetric and antisymmetric modes to the observed Raman signals in the available literature.^[31,53] Rutile is the second TiO_2 polymorph that has been detected within our soil specimens and its SERDS spectrum is characterized by two prominent Raman signals. The Ti–O symmetric stretching vibration can be found at 609 cm^{-1} , whereas the antisymmetric O–Ti–O bending vibration is located at 447 cm^{-1} .^[53–55]

It is interesting to note that titanium dioxide polymorphs can be detected within the soil matrix despite their low abundance. As determined by XRF reference analysis, the TiO_2 contents (as calculated from measured Ti elemental contents) in our studied soil specimens ranged from 0.45% to 0.78%. Fortunately, both detected polymorphs show strong Raman signals making their detection possible despite low soil titanium contents. The third TiO_2 polymorph brookite was not observed in our study, but its detection within soil has been reported previously.^[56] In this case, identification was accomplished based on the strong brookite Raman signal at 151 cm^{-1} that is not within the currently accessible spectral range of our SERDS system.

3.2.3 | Phosphates

Intrinsic phosphate species are also present in the soil and these could be identified as hydroxyapatite ($\text{Ca}_5[\text{PO}_4]_3\text{OH}$) based on the characteristic Raman signal at 962 cm^{-1} that is attributed to the symmetric P–O stretching vibration of the PO_4 group.^[15,20] This finding is in accordance with our previous Raman and SERDS studies on selected soil types where the detection of hydroxyapatite has already been demonstrated.^[5,12] This result is not surprising as all calcium orthophosphates, for example contained within commercial fertilizers, convert to hydroxyapatite in soil over time.^[9] It is important to note that the intense and spectrally broad feature above 1140 cm^{-1} in the shown SERDS spectrum of

hydroxyapatite is not a Raman signal as it does not shift with the shift in excitation wavelength as applied for SERDS. The observed band is rather due to residual contributions from intense and spectrally narrow luminescence bands that have already been observed and discussed in our previous studies on different phosphate species.^[5,57] This type of luminescence feature is likely caused by impurities due to rare earth elements and has been reported for apatites before.^[58]

3.2.4 | Carbonates

Another group of substances that has been detected and identified within our soil samples is three selected carbonates with distinct Raman spectroscopic signatures as displayed in the bottom part of Figure 2B. Aragonite (CaCO_3), calcite (CaCO_3) and dolomite ($\text{CaMg}[\text{CO}_3]_2$) exhibit their strongest Raman signal caused by the symmetric C–O stretching vibration of the CO_3 group at 1083, 1084 and 1096 cm^{-1} , respectively. Weaker contributions attributed to the in-plane bending vibration of the CO_3 group can be observed at 702 cm^{-1} (aragonite), 710 cm^{-1} (calcite) and 724 cm^{-1} (dolomite).^[11,59,60] The calcium carbonates (calcite and aragonite) can readily be distinguished from the calcium magnesium carbonate (dolomite) based on the Raman signal position of the strong CO_3 symmetric stretching vibration in the region of 1080–1100 cm^{-1} . A discrimination between the two calcium carbonate polymorphs calcite (trigonal crystal system) and aragonite (orthorhombic crystal system) can be realized considering the different spectral positions of their in-plane bending vibration of the CO_3 group around 700 cm^{-1} .

The applied SERDS raster scan approach probing 100 individual spots for each sample thus permits to recover the characteristic Raman spectroscopic signatures of in total of 13 soil constituents from intense fluorescence interference. This includes the frequently occurring species quartz and feldspars^[61–63] but also substances with low to very low abundance, for example titanium dioxide, hydroxyapatite, dolomite, zircon or diopside. Following qualitative soil analysis using SERDS, that is the identification of selected soil constituents by means of their characteristic Raman signals, the next section will deal with quantitative soil analysis. Raman spectroscopy is well-known to be suitable for quantitative measurements. In soil, however, characteristic Raman signals can be masked by fluorescence interference. Here, SERDS is a powerful tool to recover the Raman spectroscopic information to unlock the potential for quantitative measurements on soil.

3.3 | SERDS for quantitative soil carbonate determination

Calcium, for example present in the form of calcium carbonates, plays an important role within soil as it has several functions. It is essential for plants, for example serving as a pH regulator and promoting plant growth.^[64] Soil calcium content has also implications for liming requirements, for example in precision agriculture.^[65] Furthermore, calcite has been shown to be a nucleation and growth site influencing the transformation and mobility of dissolved calcium orthophosphate species in soils.^[66] For these reasons, using univariate and multivariate analysis the average SERDS spectra of each sample will be correlated with the contents of calcium carbonate as derived from the elemental calcium contents determined by XRF reference analyses to assess whether the occurring spectral variations can be used to determine this important soil parameter quantitatively.

3.3.1 | XRF reference analysis

Soil calcium contents as determined by XRF analysis served as reference values. It should be noted that XRF is an established tool to determine the total soil calcium content but is unable to determine its molecular species. Our molecule-specific SERDS study has shown the presence of five calcium-containing species in soil, namely calcite, aragonite, dolomite, hydroxyapatite and diopside, whereas another Raman study has also demonstrated the detection of calcium sulfates in Atacama Desert soil.^[56] It would therefore generally only be reasonable to correlate the total calcium amount measured by XRF with the sum of Raman signal intensities of all detected calcium species. However, from our qualitative SERDS investigations, it is known that no significant amounts of any calcium-containing molecular species other than calcium carbonate (predominantly in the form of calcite) were detected. Considering this additional molecule-specific information, it is justified to use the elemental calcium contents obtained by XRF as an estimate for the soil calcium carbonate content in our case. It is important to note that this condition is valid here but may not be applicable for other soil investigations in general where significant amounts of more than one calcium species can be present. It is therefore reasonable for our study to calculate a molecule-specific reference soil calcium carbonate content from the element-specific calcium contents determined by XRF.

3.3.2 | Univariate analysis

Based on the SERDS spectra normalized to the sapphire Raman signal at 749 cm^{-1} , the Raman signal intensities of two selected calcite Raman signals were calculated using different approaches. The determined calcium carbonate Raman signal intensities from the SERDS spectra were then correlated with the soil calcium carbonate contents derived from the XRF data. The coefficient of determination (R^2) and the root mean squared error (RMSE) were calculated as indicators of model quality.

Using the average intensity of three points around the maximum of the major calcite Raman signal at 1084 cm^{-1} , a very strong positive correlation with the reference calcium carbonate contents as calculated from soil calcium contents determined by XRF analysis ($R^2 = 0.91$) and an RMSE of 2.59% was achieved. The same calculation performed on the minor calcite Raman signal at 711 cm^{-1} revealed a slightly weaker correlation with $R^2 = 0.88$ and $\text{RMSE} = 3.09$. A small improvement can be realized when considering both Raman signals at 1084 and 711 cm^{-1} as shown in Table 1. Comparable but slightly worse correlations can be achieved when the cumulative Raman signal intensities in the spectral ranges $1076\text{--}1093\text{ cm}^{-1}$ and $705\text{--}717\text{ cm}^{-1}$ are considered rather than only average peak maximum intensities. Overall, univariate analysis considering characteristic calcite Raman signals proved to be an efficient way to assess the soil calcium carbonate content with an error rate below 3%.

3.3.3 | Partial least squares regression

Following univariate analysis based on one or two characteristic Raman signals of the target substance calcium carbonate (in the form of calcite), this section now deals with the assessment of PLSR for the prediction of the soil calcium carbonate content from the SERDS spectra. Averaged SERDS data of all 117 investigated soil samples

have been normalized to the Raman signal at 749 cm^{-1} , originating from the sapphire window used to cover the samples, and subjected to PLSR analysis.

Initially, the spectral range from 500 to 1100 cm^{-1} has been selected for the calculation of PLSR models as it contains two characteristic Raman signals of the target substance calcite (1084 and 711 cm^{-1}) and excludes the very strong Raman signal originating from quartz whose variations do not correlate well with the calcium carbonate content. A number of two PLS components have been identified by the procedure outlined in the materials and methods section and PLSR of the recorded SERDS spectra against the reference calcium carbonate contents determined from the soil calcium contents measured by XRF was performed.

A plot of the calcium carbonate content predicted from the SERDS data in dependence on the corresponding reference contents calculated from XRF data is given in Figure 3. A very good linear correlation between predicted and measured soil calcium carbonate content with a coefficient of determination of $R^2 = 0.94$ is achieved. The slope of the linear fit (dashed line) amounts to 0.96 and is very close to the ideal 1:1 relation (solid line, slope = 1.0) between predicted and measured values. The RMSECV amounts to 2.10% in this case.

In another attempt, the reduced spectral range from 500 to 1040 cm^{-1} including only the minor calcite Raman signal at 711 cm^{-1} was used as input data for the PLSR. Using the above-mentioned procedure, a number of five PLS components have been selected. The coefficient of determination shows only a minimal decrease to $R^2 = 0.93$ and also the slope of the linear fit of 0.95 is virtually identical, indicating a very good linear correlation between predicted and measured soil calcium carbonate content. Nevertheless, the RMSECV worsens with an increased value of 2.95%. Due to the exclusion of the major calcium carbonate Raman signal at 1084 cm^{-1} from the analyzed spectral range, a decreased performance compared to the previous model including both characteristic Raman signals is not surprising. It is,

TABLE 1 Overview of coefficient of determination R^2 and root mean squared error (RMSE) for selected calcite Raman signal intensities correlated with reference calcium carbonate contents as calculated from soil calcium contents determined by XRF analysis

Calculation method	Selected Raman signals	R^2	RMSE CaCO ₃ content/%
Mean intensity of three points	1084 cm^{-1}	0.91	2.59
	711 cm^{-1}	0.88	3.09
	1084 and 711 cm^{-1}	0.91	2.55
Cumulative signal intensity	1084 cm^{-1}	0.89	2.88
	711 cm^{-1}	0.86	3.31
	1084 and 711 cm^{-1}	0.90	2.73

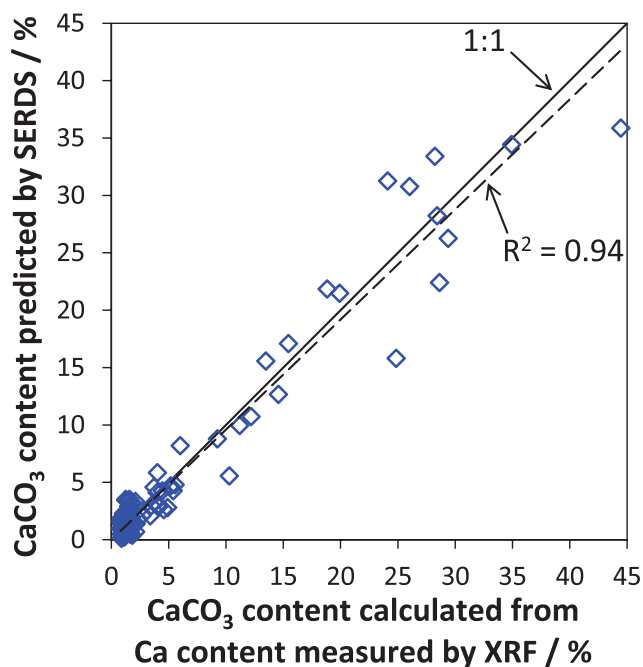


FIGURE 3 Soil CaCO_3 content predicted from SERDS spectra using PLS regression model with two components (spectral range $500\text{--}1100\text{ cm}^{-1}$) plotted in dependence of soil CaCO_3 content calculated from Ca content measured by XRF analysis. (dashed line: linear fit, solid line: 1:1 dependence) [Colour figure can be viewed at wileyonlinelibrary.com]

however, remarkable that even when only considering a minor Raman signal of the target substance, still, quantitative predictions can be realized.

An overview of selected parameters for the calculated PLS models using both or only one minor calcite Raman signal is given in Table 2. In both cases, the cumulative variance explained by the number of included PLS components is more than 92% thus capturing a large amount of the total variance present in the dataset.

To assess the spectral characteristics responsible for the obtained correlations using the PLS models, a plot of the corresponding regression coefficients for the two selected wavenumber ranges is presented in Figure 4. When the spectral region from 500 to 1100 cm^{-1} is applied, the major contribution can be found at the main calcium carbonate Raman signal at 1084 cm^{-1} whereas a smaller contribution from the second calcium carbonate Raman signal located at 711 cm^{-1} can be recognized as well. This behaviour is expected as for the prediction of calcium carbonate its characteristic Raman signals should be prominent in the regression coefficients. In this case, the regression coefficients contain the Raman signals of calcite as the most frequently detected calcium carbonate.

TABLE 2 Details of PLS regression models applied for the prediction of soil CaCO_3 content from SERDS data using spectral range containing both CaCO_3 Raman bands ($500\text{--}1100\text{ cm}^{-1}$) or spectral range comprising only the smaller CaCO_3 Raman band ($500\text{--}1040\text{ cm}^{-1}$)

Spectral range/ cm^{-1}	500–1100	500–1040
Number of components	2	5
Variance explained/%	94.5	92.7
R^2	0.94	0.93
Slope of linear fit	0.96	0.95
RMSECV/%	2.10	2.95

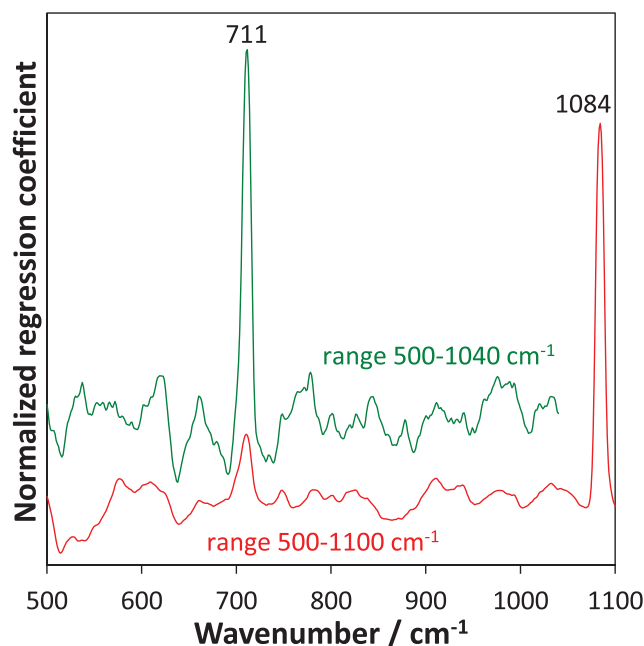


FIGURE 4 Regression coefficients of separate PLS models with two components (spectral range $500\text{--}1100\text{ cm}^{-1}$) and five components (spectral range $500\text{--}1040\text{ cm}^{-1}$) used to predict soil CaCO_3 content from SERDS spectra. Coefficients were normalized to their respective maximum and vertically offset for clarity. [Colour figure can be viewed at wileyonlinelibrary.com]

When the truncated range from 500 to 1040 cm^{-1} without the main calcium carbonate Raman signal is used for the regression, the dominant contribution arises from the remaining calcium carbonate Raman signal at 711 cm^{-1} that is attributed to calcite. In both cases, characteristic Raman signals of the predicted target substance calcium carbonate (present as calcite polymorph) dominate the corresponding regression coefficients, and no further strong contributions from other molecular species can be observed.

It should be noted that PLS considers spectral contributions of all soil constituents with Raman signals being located in the analyzed spectral range (this also includes the strongest Raman signals of all five identified calcium-containing species: calcite, aragonite, dolomite, hydroxyapatite and diopside) and tries to correlate their variations with variations present in the reference CaCO_3 contents (as calculated from XRF data). Here, the outcome is that calcite plays the dominant role in the carbonate content prediction, whereas the other four calcium-containing species do not play a major role due to their much lower abundance in the soil. Overall, the molecule-specific information derived from the SERDS data is well suited for the quantitative assessment of the soil calcium carbonate content.

In the following, a brief comparison of the performance of univariate and multivariate models for calcium carbonate prediction in the set of investigated soil samples will be given. For univariate analysis, the best prediction could be realized using the sum of mean intensities of both calcite Raman bands (1084 and 711 cm^{-1}) with $R^2 = 0.91$ and $\text{RMSE} = 2.55\%$. When considering only the mean intensity of the minor Raman signal at 711 cm^{-1} , according to expectations, the performance decreases to $R^2 = 0.88$ and $\text{RMSE} = 3.09\%$. In the case of multivariate PLSR, values of $R^2 = 0.94$ and $\text{RMSECV} = 2.10\%$ were achieved when considering both calcite Raman signals while the model based only on the minor Raman signal at 711 cm^{-1} led to inferior values of $R^2 = 0.93$ and $\text{RMSECV} = 2.95\%$. It is noteworthy that a simple univariate analysis based on Raman signal intensities performs only slightly worse than PLSR. This observation can be explained by the fact that the main contributions in the multivariate regression coefficients are actually limited to the spectral regions containing the two Raman signals of the target substance calcium carbonate (present as calcite polymorph). Thus, Raman band intensities, as well as integrated band intensities/areas within a specific wavenumber range, can provide a suitable measure for the prediction of the soil calcium carbonate content.

3.4 | Spatial distribution of calcium carbonate

As mentioned above, the soil samples were collected at equidistant intervals of 24 m covering a total length of 624 m across the agricultural field and also considering selected depths below the soil surface down to 1 m . From the predicted calcium carbonate contents using PLSR, it is therefore possible to visualize the spatial distribution of calcium carbonate across the field and with respect to soil

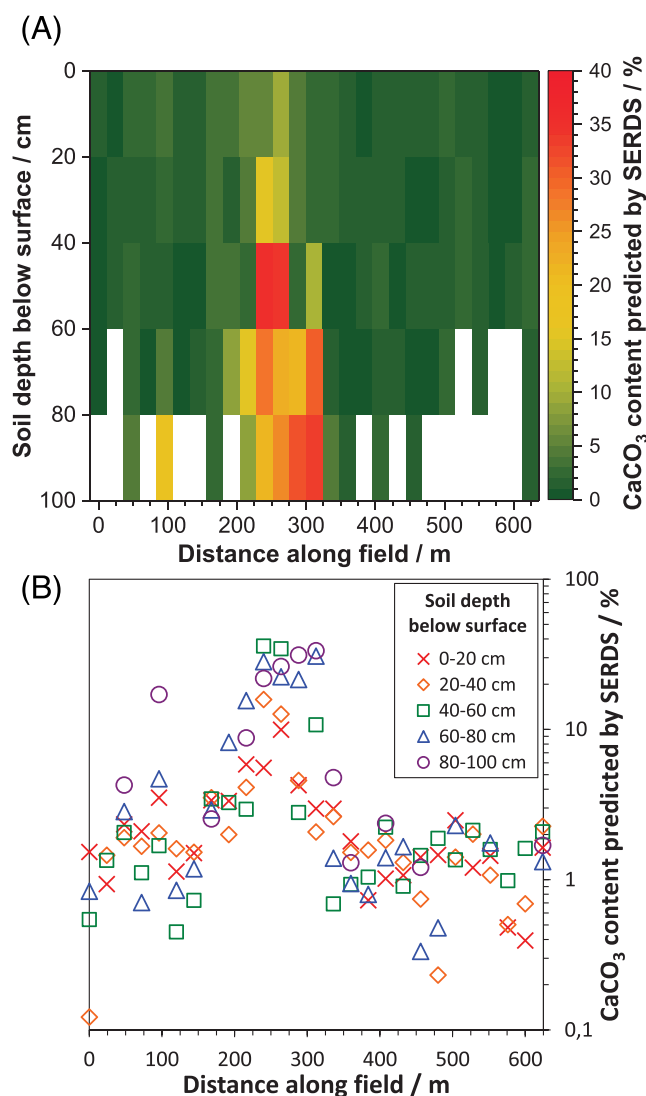


FIGURE 5 Spatial distribution of CaCO_3 content predicted from SERDS spectra using PLS regression (model with two components in the spectral range $500\text{--}1100\text{ cm}^{-1}$) plotted in dependence of the distance along the field for different sampling depths below the soil surface, false-color plot (A) and logarithmic CaCO_3 content plots for individual depth layers (B). White bars in (A) indicate positions where no sample was collected. [Colour figure can be viewed at wileyonlinelibrary.com]

depth (see Figure 5). Due to the natural and man-made soil heterogeneity at the field scale,^[67] the occurrence of calcium carbonate is not evenly distributed along the investigated length scales. For the majority of sampling positions, the calcium carbonate content is well below 5%, mostly irrespective of the investigated soil depth. There is, however, an area around the center of the field with elevated concentrations, roughly between 200 and 320 m as measured from the starting point. In this range, the highest concentrations of up to 36% can be found in the subsoil layers at depths below 40 cm, whereas the

upper soil layers exhibit maximum concentrations in the range of 10%–15%.

The present spatial heterogeneity, even between adjacent points at 24 m distance away from each other, highlights the need for advanced sensing techniques to adequately capture such variations. Currently applied soil inspection procedures in many countries are mostly based on the collection of one mixed sample from large areas up to 3 ha^[65] and subsequent standard laboratory analysis. This means that neighboring sampling points are separated by distances on the order of 100 m or more. Unfortunately, due to the time-consuming and expensive nature of conventional laboratory analysis,^[68] an increase in the number of samples to be collected is not practically feasible. A potential solution could be the application of portable sensing systems for the on-site acquisition of soil parameters. As demonstrated in this paper, SERDS is a powerful technique for qualitative and quantitative soil analysis. To further evaluate the potential of the technique in the context of precision agriculture, a portable SERDS system has been developed by our group and was successfully tested in a field trial.^[69]

4 | CONCLUSIONS

SERDS in combination with a raster scan approach has been demonstrated as a suitable tool for qualitative and quantitative soil analysis. Within a diverse set of soil samples, the method enabled the detection and identification of in total 13 mineral soil constituents. Based on the Raman spectroscopic fingerprint extracted from intense fluorescence interference by SERDS, discrimination between closely related molecular species including polymorphic forms of titanium dioxide and calcium carbonate could be realized. Within a set of 117 soil samples collected from an agricultural field along a distance of more than 600 m and down to depths of 1 m, the spectroscopic information derived by SERDS could be used for quantitative soil analysis as well. Both univariate and multivariate approaches showed very good performance for the prediction of the calcium carbonate content as an important soil parameter.

The results highlight the large potential of SERDS as a promising tool for soil analysis in precision agriculture opening new avenues for efficient soil nutrient management. Besides the agricultural sector, further application areas could benefit from the capabilities of SERDS for substance identification and quantification as well. Examples include geological studies, for example for mineral characterization on planetary surfaces^[38,70] and the

field of cultural heritage, for example for archeological studies^[71,72] or investigations of deterioration effects on monuments.^[73,74]

ACKNOWLEDGEMENTS

The research leading to these results received funding from the Federal Ministry of Education and Research (BMBF) under Grant Agreement No. 031B0513C. This work is realized within the project RaMBo (Raman-Messsystem zur ortsspezifischen Bodenanalytik) within the consortium I4S (Intelligence for Soil) in the frame of the funding measure BonaRes (Soil as a Sustainable Resource for the Bioeconomy). The study was also partially funded by the BMBF under Grant Agreement No. FMD 16FMD02 (Research Fab Microelectronics Germany—FMD). We would like to thank all involved colleagues from I4S for sample collection and preparation, and the landowner Golo Philipp for access to the agricultural field. We are particularly grateful to Maria Krichler (Ferdinand-Braun-Institut, Leibniz-Institut für Höchstfrequenztechnik) for developing the software to control the experimental setup. Open Access funding enabled and organized by Projekt DEAL.

CONFLICTS OF INTEREST

None.


DATA AVAILABILITY STATEMENT

The data that support the findings of this study are available from the corresponding author upon reasonable request.

ORCID

Kay Sowoidnich  <https://orcid.org/0000-0002-7173-2677>

Martin Maiwald  <https://orcid.org/0000-0003-1166-5529>

Markus Ostermann  <https://orcid.org/0000-0001-8116-5808>

Bernd Sumpf  <https://orcid.org/0000-0001-5044-955X>

REFERENCES

- [1] I. Bhakta, S. Phadikar, K. Majumder, *J. Sci. Food Agric.* **2019**, 99, 4878.
- [2] S. Armenta, M. De la Guardia, *Trends Environ. Anal. Chem.* **2014**, 2, 43.
- [3] M. Debeljak, A. Trajanov, V. Kuzmanovski, J. Schröder, T. Sandén, H. Spiegel, D. P. Wall, M. Van de Broek, M. Rutgers, F. Bampa, R. E. Creamer, C. B. Henriksen, *Front. Environ. Sci.* **2019**, 7, 115.
- [4] J. Kruse, M. Abraham, W. Amelung, C. Baum, R. Bol, O. Kühn, H. Lewandowski, J. Niederberger, Y. Oelmann, C. Rüger, J. Santner, M. Siebers, N. Siebers, M. Spohn, J. Vestergren, A. Vogts, P. Leinweber, *J. Plant Nutr. Soil Sci.* **2015**, 178, 43.

- [5] P. M. Nkebiwe, K. Sowoidnich, M. Maiwald, B. Sumpf, T. E. Hartmann, D. Wanke, T. Müller, *J. Plant Nutr. Soil Sci.* **2022**, *185*, 221.
- [6] H. Edwards, T. Munshi, I. Scowen, A. Surtees, G. T. Swindles, *J. Raman Spectrosc.* **2012**, *43*, 323.
- [7] K. Ikehata, Y. Arakawa, J. I. Ishibashi, *Vib. Spectrosc.* **2021**, *114*, 103247.
- [8] A. Wang, J. Wei, R. L. Korotev, *J. Raman Spectrosc.* **2020**, *51*, 1636.
- [9] C. Vogel, C. Adam, R. Sekine, T. Schiller, E. Lipie, D. McNaughton, *Appl. Spectrosc.* **2013**, *67*, 1165.
- [10] B. W. Kammrath, A. Koutrakos, J. Castillo, C. Langley, D. Huck-Jones, *Forensic Sci. Int.* **2018**, *285*, e25.
- [11] Z. Tomić, P. Makreski, B. Gajić, *J. Raman Spectrosc.* **2010**, *41*, 582.
- [12] L. S. Theurer, M. Maiwald, B. Sumpf, *Eur. J. Soil Sci.* **2021**, *72*, 120.
- [13] Z. Xing, C. Du, K. Tian, F. Ma, Y. Shen, J. Zhou, *Talanta* **2016**, *158*, 262.
- [14] D. V. de Sousa, J. C. Ker, C. E. R. Schaefer, M. J. Rodet, L. M. Guimarães, J. F. Felix, *Catena* **2018**, *171*, 552.
- [15] A. M. Lanfranco, P. F. Schofield, P. J. Murphy, M. E. Hodson, J. F. W. Mosselmans, E. Valsami-Jones, *Mineral. Mag.* **2003**, *67*, 1299.
- [16] K. Sowoidnich, S. Vogel, M. Maiwald, B. Sumpf, *Appl. Spectrosc.* **2022**, *76*, 712.
- [17] C. Vogel, J. Helfenstein, M. S. Massey, R. Sekine, R. Kretzschmar, L. Beiping, T. Peter, O. A. Chadwick, F. Tamburini, C. Rivard, H. Herzog, C. Adam, A. E. Pradas del Real, H. Castillo-Michel, L. Zuin, D. Wang, R. Félix, B. Lassalle-Kaiser, E. Frossard, *Geoderma* **2021**, *381*, 114681.
- [18] T. R. Schlack, S. A. Beal, E. J. Corriveau, J. L. Clausen, *ACS Omega* **2021**, *6*, 16316.
- [19] A. S. Luna, I. C. A. Lima, W. F. C. Rocha, J. R. Araújo, A. Kuznetsov, E. H. M. Ferreira, R. Boqué, J. Ferré, *Anal. Methods* **2014**, *6*, 8930.
- [20] C. Vogel, M. Ramsteiner, R. Sekine, A. Doolette, C. Adam, *J. Raman Spectrosc.* **2017**, *48*, 867.
- [21] A. P. Shreve, N. J. Cherepy, R. A. Mathies, *Appl. Spectrosc.* **1992**, *46*, 707.
- [22] J. Zhao, M. M. Carrabba, F. S. Allen, *Appl. Spectrosc.* **2002**, *56*, 834.
- [23] M. Maiwald, A. Müller, B. Sumpf, G. Tränkle, *J. Raman Spectrosc.* **2016**, *47*, 1180.
- [24] M. Maiwald, A. Müller, B. Sumpf, G. Erbert, G. Tränkle, *Appl. Opt.* **2015**, *54*, 5520.
- [25] B. Sumpf, M. Maiwald, A. Müller, J. Fricke, P. Ressel, F. Bugge, G. Erbert, G. Tränkle, *Appl. Phys. B: Lasers Opt.* **2015**, *120*, 261.
- [26] S. De Jong, *Chemom. Intell. Lab. Syst.* **1993**, *18*, 251.
- [27] C. M. Andersen, R. Bro, *J. Chemom.* **2010**, *24*, 728.
- [28] J. Jehlička, P. Vitek, H. G. M. Edwards, M. Heagraves, T. Čapoun, *Spectrochim. Acta - Part a Mol. Biomol. Spectrosc.* **2009**, *73*, 410.
- [29] D. T. M. Phan, T. Häger, W. Hofmeister, *J. Raman Spectrosc.* **2017**, *48*, 453.
- [30] W. Zhu, G. Pezzotti, *J. Appl. Phys.* **2011**, *109*, 073502.
- [31] M. A. Boda, M. A. Shah, *Mater. Res. Express* **2017**, *4*, 075908.
- [32] C. Carey, T. Boucher, S. Mahadevan, P. Bartholomew, M. D. Dyar, *J. Raman Spectrosc.* **2015**, *46*, 894.
- [33] S. T. Ishikawa, V. C. Gulick, *Comput. Geosci.* **2013**, *54*, 259.
- [34] J. L. White, *Soil Sci.* **1971**, *112*, 22.
- [35] M. Veneranda, J. A. Manrique-Martinez, C. Garcia-Prieto, A. Sanz-Arranz, J. Saiz, E. Lalla, M. Konstantinidis, A. Moral, J. Medina, F. Rull, L. M. Nieto, G. Lopez-Reyes, *Icarus* **2021**, *367*, 114542.
- [36] V. Fuertes de la Llave, A. del Campo, J. F. Fernández, E. Enríquez, *J. Raman Spectrosc.* **2019**, *50*, 741.
- [37] I. Aliatis, E. Lambruschi, L. Mantovani, D. Bersani, S. Andò, G. Diego Gatta, P. Gentile, E. Salvioli-Mariani, M. Prencipe, M. Tribaudino, P. P. Lottici, *J. Raman Spectrosc.* **2015**, *46*, 501.
- [38] J. J. Freeman, A. Wang, K. E. Kuebler, B. L. Jolliff, L. A. Haskin, *Can. Mineral.* **2008**, *46*, 1477.
- [39] S. Endo, M. Nagashima, M. Enami, *J. Mineral. Petrol. Sci.* **2019**, *114*, 161.
- [40] P. Makreski, G. Jovanovski, S. Stojančeska, *J. Mol. Struct.* **2005**, *744–747*, 79.
- [41] Y. V. Bataleva, A. N. Kruk, I. D. Novoselov, Y. N. Palyanov, *Minerals* **2020**, *10*, 1.
- [42] J. Dong, Y. Han, J. Ye, Q. Li, S. Liu, D. Gu, *J. Raman Spectrosc.* **2014**, *45*, 596.
- [43] S. Kos, M. Dolenc, J. Lux, S. Dolenc, *Minerals* **2020**, *10*, 325.
- [44] B. Härtel, R. Jonckheere, B. Wauschkuhn, L. Ratschbacher, *Geochronology* **2021**, *3*, 259.
- [45] A. E. Maftai, A. Buzatu, G. Damian, N. Buzgar, H. G. Dill, A. I. Apopei, *Minerals* **2020**, *10*, 988.
- [46] A. J. Anderson, J. M. Hanchar, K. V. Hodges, M. C. van Soest, *Chem. Geol.* **2020**, *538*, 119494.
- [47] B. A. Kolesov, C. A. Geiger, T. Armbruster, *Eur. J. Mineral.* **2001**, *13*, 939.
- [48] M. Zhang, E. K. H. Salje, I. Farnan, A. Graeme-Barber, P. Daniel, R. C. Ewing, A. M. Clark, H. Leroux, *J. Phys. Condens. Matter* **1915**, *2000*, 12.
- [49] P. Richet, B. O. Mysen, J. Ingrin, *Phys. Chem. Miner.* **1998**, *25*, 401.
- [50] M. Prencipe, L. Mantovani, M. Tribaudino, D. Bersani, P. P. Lottici, *Eur. J. Mineral.* **2012**, *24*, 457.
- [51] M. Tribaudino, L. Mantovani, D. Bersani, P. Lottici, *Am. Mineral.* **2012**, *97*, 1339.
- [52] U. Diebold, *Surf. Sci. Rep.* **2003**, *48*, 53.
- [53] A. J. Pinto, N. Sanchez-Pastor, I. Callegari, B. Pracejus, A. Scharf, *Sci. Rep.* **2020**, *10*, 7445.
- [54] I. Lukačević, S. K. Gupta, P. K. Jha, D. Kirin, *Mater. Chem. Phys.* **2012**, *137*, 282.
- [55] Y. Zhang, C. X. Harris, P. Wallenmeyer, J. Murowchick, X. Chen, *J. Phys. Chem. C* **2013**, *117*, 24015.
- [56] J. Wei, A. Wang, J. L. Lambert, D. Wettergreen, N. Cabrol, K. Warren-Rhodes, K. Zacny, *J. Raman Spectrosc.* **2015**, *46*, 810.
- [57] K. Sowoidnich, M. Oster, K. Wimmers, M. Maiwald, B. Sumpf, *J. Raman Spectrosc.* **2021**, *52*, 1418.
- [58] A. Culka, J. Jehlička, *J. Raman Spectrosc.* **2018**, *49*, 526.
- [59] L. Borromeo, U. Zimmermann, S. Andò, G. Coletti, D. Bersani, D. Basso, P. Gentile, B. Schulz, E. Garzanti, *J. Raman Spectrosc.* **2017**, *48*, 983.
- [60] M. L. Frezzotti, F. Tecce, A. Casagli, *J. Geochem. Explor.* **2012**, *112*, 1.

- [61] D. C. Bain, A. Mellor, M. S. E. Robertson-Rintoul, S. T. Buckland, *Geoderma* **1993**, *57*, 275.
- [62] V. L. Mulder, M. Plötze, S. de Bruin, M. E. Schaepman, C. Mavris, R. F. Kokaly, M. Egli, *Geoderma* **2013**, *207–208*, 279.
- [63] A. Kabata-Pendias, *Appl. Geochemistry* **1993**, *8*, 3.
- [64] M. Rühlmann, D. Büchele, M. Ostermann, I. Bald, T. Schmid, *Spectrochim. Acta - Part B at. Spectrosc.* **2018**, *146*, 115.
- [65] M. Leenen, G. Welp, R. Gebbers, S. Pätzold, *J. Plant Nutr. Soil Sci.* **2019**, *182*, 953.
- [66] L. Wang, E. Ruiz-Agudo, C. V. Putnis, M. Menneken, A. Putnis, *Environ. Sci. Technol.* **2012**, *46*, 834.
- [67] S. Pätzold, F. M. Mertens, L. Bornemann, B. Koleczek, J. Franke, H. Feilhauer, G. Welp, *Precis. Agric.* **2008**, *9*, 367.
- [68] R. A. Viscarra Rossel, A. B. McBratney, *Aust. J. Exp. Agric.* **1998**, *38*, 765.
- [69] M. Maiwald, K. Sowoidnich, B. Sumpf, *J. Raman Spectrosc.* **2022**, *53*, 1560.
- [70] E. A. Lalla, M. Konstantinidis, G. Lopez-Reyes, M. G. Daly, M. Veneranda, J. A. Manrique, G. Groemer, J. L. Vago, F. Rull, *J. Raman Spectrosc.* **2020**, *51*, 2525.
- [71] D. Bersani, P. P. Lottici, *J. Raman Spectrosc.* **2016**, *47*, 499.
- [72] M. J. Ayora-Cañada, A. Domínguez-Arranz, A. Dominguez-Vidal, *J. Raman Spectrosc.* **2012**, *43*, 317.
- [73] I. Ibarrondo, U. Balziskueta, I. Martínez-Arkarazo, C. García-Florentino, G. Arana, A. Azkarate, J. M. Madariaga, *J. Raman Spectrosc.* **2021**, *52*, 109.
- [74] S. Kramar, M. Urosevic, H. Pristacz, B. Mirtič, *J. Raman Spectrosc.* **2010**, *41*, 1441.

How to cite this article: K. Sowoidnich, M. Maiwald, M. Ostermann, B. Sumpf, *J Raman Spectrosc* **2023**, *1*. <https://doi.org/10.1002/jrs.6500>